OPEN ACCESS
IOP Publishing
Superconductor Science and Technology
Supercond. Sci. Technol. **31** (2018) 013001 (15pp)
https://doi.org/10.1088/1361-6668/aa9882

Topical Review

Radiation effects on iron-based superconductors

M Eisterer

Atominstitut, TU Wien, Stadionallee 2, A-1020 Vienna, Austria

E-mail: michael.eisterer@tuwien.ac.at

Received 28 July 2017, revised 3 November 2017
Accepted for publication 6 November 2017
Published 5 December 2017

Abstract

This article reviews the results of irradiation experiments on iron-based superconductors, with particular emphasis on neutron irradiation. These experiments were either done to foster the theoretical understanding of superconductivity in these compounds by investigating the influence of impurity scattering on the fundamental superconducting properties or to investigate vortex physics and to benchmark flux pinning in view of applications. Results on the most explored iron-based compounds are summarized and compared with data on metallic superconductors, cuprates, and MgB_2. Similarities and differences are discussed as well as the influence of the type and energy of the particles used for the experiments.

Keywords: irradiation, iron-based superconuctors, disorder effects, critical currents

(Some figures may appear in colour only in the online journal)

1. Introduction

The introduction of defects by means of irradiation techniques offers the unique possibility to investigate changes to superconducting properties caused by additional defects without the problems of sample-to-sample variation, because the same sample can be investigated before and after irradiation. Moreover, the defects can be produced in all compounds rather easily and a very similar defect structure is created in many cases, which enables a comparison of different materials. The introduced defect structure can be chosen by the type of the irradiating particle and its energy. Small defects which enhance the scattering rate of the charge carriers can be used to perform fundamental studies on superconductors, e.g. to check predictions about the influence of enhanced scattering on the superconducting gaps, the transition temperature or the superfluid density. For instance the transition from two-gap to single gap superconductivity by enhanced scattering following neutron irradiation was demonstrated in MgB_2 [1]. In the iron-based superconductors, enhanced scattering provides information on the gap symmetry, a possible sign reversal or nodes in the gap. Larger defects can act as efficient pinning centers for vortices enhancing the critical currents or diminishing flux creep. Irradiation experiments also benchmark the achievable critical currents in a superconducting compound and indicate the necessity of improving pinning to enhance their application potential [2–4]. Recently, it was even demonstrated that ion irradiation can be used for improving the critical current in coated conductors on an industrial scale [5, 6]. Granularity effects can be studied by tuning the ratio between the currents flowing within the grains and the currents crossing grain boundaries [7–9]. Finally, irradiation experiments have been also carried out to test the suitability of a conductor for operation in a radiation environment, such as fusion [10–12] or accelerator magnets [13, 14]. The aim of this topical review is to summarize these different kinds of irradiation experiments on iron-based superconductors and compare them with other superconducting materials. The article is structured as follows: after a short summary of the defect structure resulting from irradiation with different particles and energies, the influence of the enhanced scattering on fundamental superconducting

parameters (gap, superfluid density, transition temperature, upper critical field) of the iron superconductors will be reviewed. Finally results on the changes in vortex pinning will be discussed.

2. Radiation damage and defect structure

Radiation induced defects result in increased scattering (or a reduced quasi-particle lifetime) which is generally of non-magnetic nature in the iron-based superconductors. Only in Nd-1111 (NdFeAsO) Kondo-like defects sites were found after irradiation with α-particles [15]. Although all defects enhance scattering, a high density of point-like defects is most efficient. Point-like defects are generated by all irradiation techniques discussed in this paper, they are often accompanied by larger defects. Electron irradiation at low temperature is best suited to generate only Frenkel pairs, i.e. a vacancy and an interstitial. Larger defects (nm sized) on the other hand, are more efficient for pinning, especially at high temperatures.

2.1. Charged particles

Irradiation experiments on superconducting materials have been performed with a variety of particles, their rest masses ranging from about 0.5 MeV/c (electrons) to around 220 GeV/c (U, Au, Pb ions) and kinetic energies from a few keV to GeV. Charged particles transfer this energy to matter either by interactions via the electronic system or by collisions with the nuclei of the lattice. The electronic stopping power (S_e) dominates for high energy charged particles, while the nuclear collisions contribute the most to the energy loss (S_n) at low energies. S_e generally increases with the particle mass but is non-monotonous in energy. It has a maximum near the end of the particle's trajectory (Bragg peak), where the kinetic energy is comparatively small. Parallel continuous columnar defects with a diameter of a few nanometer resulting from local melting are generated at high stopping power (S_e exceeding about 30 MeV μm^{-1} in the cuprates) [16], which become splayed at lower stopping power and their diameter is no longer constant along the trajectory. The defects become discontinuous upon a further reduction of S_e (e.g. 200 MeV Au [17, 18] or 1.4 GeV Pb [19] ions in Ba-122 ($BaFe_2As_2$)), defects elongated along the trajectory and finally nearly spherical defects of a few nanometers are formed [20, 21] which become smaller and irregularly shaped with decreasing stopping power [16]. Electrons for instance, produce only atomic disorder by displacing single atoms. (2.5 MeV electrons create about 4.2×10^{25} Frenkel pairs [22] at a fluence of 10^{23} m^{-2}.) The penetration depth of heavy charged particles in matter is typically of the order of 20–30 μm, only light particles with very high energies (e.g. electrons or protons) penetrate much deeper (centimeter to meter). The defects created by high energy ions at a given energy loss rate seem to be smaller in the iron-based superconductors than in the cuprates. Segmented columnar defects with a diameter of around 4 nm were reported in Ba-122 after irradiation with 1.4 GeV Pb ions [19] or 200 MeV Ag-ions [18], while continuous columnar defects of 6–8 nm in diameter result from such particles in the cuprates. Continuous columnar defects were observed in Nd-1111 after irradiation with 2 GeV Ta-ions [23]. Tamegai *et al* calculated the energy loss of some ions in Ba-122, e.g. 28 MeV μm^{-1} and 47.7 MeV μm^{-1} for 200 MeV Au ions and 2.6 GeV U-ions, respectively. Slightly higher values were obtained for the 11 ($FeSe_{1-x}Te_x$) system. On the other hand the number of displaced atoms after 3 MeV proton irradiation was calculated to be 8.7×10^{-4} in Ba-122 [24] and only 2.7×10^{-4} in Y-123 [20].

2.2. Neutrons

Since neutrons are not charged, i.e. $S_e = 0$, they interact only via nuclear collisions or reactions. While charged particles normally have a well defined energy in irradiation experiments, which is defined by the accelerator, neutron sources typically provide neutrons having a wide energy distribution. In a fission reactor, the neutron energies can be roughly divided into three groups: fast neutrons from the fission reaction having energies between about 0.1 and 10 MeV, thermal neutrons with a Maxwell–Boltzmann energy distribution peaking at about 40 meV and so-called epithermal neutrons at intermediate energies, representing moderated neutrons which are not fully thermalized [25]. Defects can be generated by elastic collisions only if the transferred energy exceeds the binding energy of the lattice atom (typically a few eV in metals and 10–40 eV in ionic crystals), which is maximally (central collision) $\frac{4m_L m_n}{(m_L+m_n)^2}E_n$. m_L and m_n denote the mass of the lattice atom and the neutron, respectively. E_n refers to the energy of the incident neutron. Materials containing light elements thus suffer more damage from elastic collisions than compounds made up of heavy elements. From this point of view, the cuprates may become more disordered than most other compounds, since they contain a large amount of oxygen. The realistic minimum energy where defect production due to collisions sets in is about 100 eV, thus thermal neutrons do not produce any defects by elastic collisions. If the transferred energy is much higher than the binding energy (the threshold being of the order of 1 keV), the displaced atom collides with other lattice atoms leading to an avalanche-like defect production, which locally melts the lattice. A so-called collision cascade is formed, a spherical defect with a diameter of about 5 nm [26]. The collision cascades are statistically distributed and the penetration depth of fast neutrons amounts to tens of centimeters in many materials, ensuring a homogeneous defect structure also in bulk samples. Since the fast neutrons are most efficient for producing this kind of defects, their density is roughly proportional to the fast neutron fluence, but depends on details of the high-energy neutron distribution. (For the TRIGA reactor of the Atominstitut in Vienna, it is approximately 5 m^{-1} times the fast neutron fluence, which corresponds to a mean free path of 20 cm.) High and medium energy neutrons also produce smaller defects, down to single displaced atoms and interstitials. For instance, copper–oxygen divacancies were found in the cuprates [27]. Unlike the density of collision cascades, their density does not scale with fluence and is

much larger than the density of the collisions cascades at low neutron fluence. In the metallic superconductors, the larger thermal conductivity inhibits local melting during the displacement cascade and clouds or clusters of point defects are formed instead of the collision cascades. In the iron-based superconductors on the other hand, one expects a similar defect structure as in the cuprates, although an experimental confirmation is still lacking.

2.3. Nuclear reactions

Neutrons or protons react with lattice nuclei resulting in fission of the nucleus or absorption of the neutron followed by the emission of γ-radiation or particles. For instance, the ^{209}Bi nuclei of $Bi_2Sr_2CaCu_2O_8$ (Bi-2212) are fissioned by 0.8 GeV protons [28]. Different reaction products can occur with mass numbers around 100 and energies of the order of 100 MeV. These products are just heavy ions of high energy and produce columnar defects with a diameter of 7 nm [28]. These defects are randomly oriented, in contrast to heavy ion irradiation, where the defects are more or less parallel to the incident beam. A similar defect structure was introduced into $YBa_2Cu_3O_{7-\delta}$ (Y-123) by the addition of uranium which was subsequently fissioned by thermal neutrons [29, 30]. Neutron absorption reactions are relevant for the neutron irradiation of $GdBa_2Cu_3O_{7-\delta}$ (Gd-123) or MgB_2. The neutron absorption by Gd is followed by a γ-emission, whose recoil is just sufficient to displace the Gd-nucleus. The effect of these point defects on T_c is nevertheless dramatic, since the corresponding reaction cross section is huge [11]. An α-particle with an energy of 1.7 MeV is emitted after neutron absorption by ^{10}B, which subsequently causes defect cascades in MgB_2 [31]. To the best of the author's knowledge, no irradiation experiments relying on nuclear reactions within the superconductor have been reported for iron-based superconductors yet. Although neutron capture reactions may play a role in neutron irradiation experiments, for instance neutron capture by Sm in SmFeAsO (Sm-1111) [32], clear evidence does not exist so far.

3. Fundamental properties

Defects resulting in isotropic scattering are usually desired for the investigation of changes of the fundamental materials properties due to increased scattering. With the naive picture that isotropic scattering reduces the anisotropy of all properties, most of the observed changes can be understood, e.g. the change of the gap symmetry, the decrease in T_c, or the reduction of the upper critical field anisotropy.

3.1. Pairing symmetry

The pairing symmetry is of primary importance for a theoretical description of unconventional superconductors. Although angle-resolved photoemission spectroscopy enables a direct assessment of the energy gap and its anisotropy in different bands within experimental resolution, it is not possible to extract a possible sign reversal or to exclude surface effects. The gap symmetry is thus often addressed indirectly, for instance by the temperature dependence of the superfluid density [33–36], THz spectroscopy [37], thermal conductivity [38–40] or by the influence of disorder on the transition temperature [15, 41–45]. Disorder potentially changes the pairing symmetry by making the gap more isotropic, reducing its largest value (which in turn decreases T_c) and (sometimes) enhancing its minima. This was demonstrated for MgB_2, where neutron irradiation progressively reduced the larger gap until it merged with the small one [1]. In most of the iron-based compounds, s_{+-}-pairing symmetry resulting from antiferromagnetic spin-fluctuations is a popular scenario [46], although still under debate. The difference to the s_{++} symmetry prevailing in MgB_2 is a changing sign between the (at least) two (nearly isotropic) gaps on different sheets of the Fermi surface. Schilling *et al* [37] claimed a transformation form s_{+-} to s_{++} symmetry in Co-doped Ba-122 by disorder resulting from 200 keV proton irradiation, as predicted theoretically [47]. Accidental nodes in the order parameter may be lifted by disorder [48] consistent with results of electron irradiation experiments on phosphorous-doped Ba-122 [33, 49] or Sr-122 [35] within the s_{+-} scenario. The authors of the latter two studies did not find evidence for a transition to s_{++} symmetry in these compounds.

The decrease of the transition temperature after various irradiation experiments, which is discussed in the next subsection, seemed to be too small for s_{+-} pairing at first glance in $Ca_{0.5}Na_{0.5}Fe_2As_2$ [42], Co-[43] or K-doped [36] Ba-122, Nd-1111 [15], and La-1111 [41]. Kim *et al* [42] argued that the Abrikosov–Gorkov theory, on which the prediction is based, breaks down and has to be replaced by a Swiss cheese model [50], but the main problem is the difficulty to determine the inter-band scattering rate experimentally, which is the relevant parameter for the T_c-reduction [47, 48, 51, 52] in a multi-band conductor. Since the influence of disorder on T_c may be similar for d-wave or s_{+-} pairing [51], one may end up with the conclusion that probing the gap symmetry by disorder is not as decisive as in the cuprates [53]. Indeed, consistency with s_{+-} pairing has been found in $Ba(Fe_{0.76}Ru_{0.24})_2As_2$ after electron irradiation by a proper choice of the parameters [44]. Alternative explanations for a weaker sensitivity of T_c to disorder were given by the influence of quantum criticality [54] or the weakening of the competing magnetic order [55].

3.2. Transition temperature

Non-magnetic scattering is not pair breaking in single band s-wave superconductors and thus does not change the transition temperature. Changes in T_c after irradiation, therefore, either result from non-conventional superconductivity (including anisotropy of the order parameter) or from second order effects such as changes in the electronic density of states (DOS). Inter-band scattering between different bands or intra-band scattering in bands with anisotropic gaps (e.g. d-wave) do not preserve the energy of the particle and consequently reduce T_c [47, 48, 51, 52]. However, pair breaking and a reduction of the

superconducting energy gap are not the only possible reasons for a T_c-reduction caused by irradiation. The newly created defects cause strain and change the lattice parameter, which in turn can lead to a change in the electronic DOS. Strong intraband scattering can change the DOS as well by smearing the Fermi surface [56, 57]. A change of the relevant phonon energy may contribute to a change of T_c in BCS superconductor, a possible influence of disorder on antiferromagnetic spin fluctuation is, to the best of the author's knowledge, currently unclear.

A decrease in transition temperature has been reported in the vast majority of irradiation experiments on iron-based superconductors. Only one study known to the author reports an unchanged T_c of K-doped Ba-122 up to a fluence of $10^{16}\,m^{-2}$ (1.4 GeV Pb irradiation) [34]. However, other reports claimed a small decrease [19, 58]. The observed *increase* of T_c in the $FeSe_{1-x}Te_x$ system [22, 59, 60] and in under-doped Ba-122 [61] will be discussed below. An overview of available literature data is given in table 1.

Neutron irradiation in a fission reactor has a similar effect on the transition temperature in all investigated iron-based superconductors except $FeSe_{1-x}Te_x$. A decrease of $1–2 \times 10^{-22}\,Km^2$ was found for Co-, P-, and K-doped Ba-122, and for Nd- and Sm-1111. This value refers to samples close to optimal doping. It is smaller than the respective decrease in the cuprates (e.g., 2.3×10^{-22} Km^2 in coated conductors [10, 62] or about 4×10^{-22} Km^2 in single crystals [63, 64]), where nodes in the gap function are well-established due to *d*-wave symmetry. A significantly smaller decrease rate was found in Nb_3Sn (0.35×10^{-22} Km^2) [13], which is a fully gaped superconductor and a decrease in the electronic DOS at the Fermi level is responsible in that case. However, although a comparison of the changes induced by a particular radiation is useful for testing the suitability of a certain material in the respective environment (fusion [10, 62] or accelerator magnets [14, 65, 66]), it is a bit problematic for a comparison of the material's sensitivity to disorder for drawing conclusions on the underlying mechanisms, since the introduced disorder itself depends on the material. The number of displacements per atom (dpa) is a more suitable measure for this purpose, although the morphology of the defects is expected to be important as well with single displaced atoms being the most efficient scattering centers and hence reducing the transition temperature the most at a given dpa. However, the transition temperature scaled quite well with the number of displaced atoms in Nb_3Sn irrespective of the particle type (neutrons and protons) and energy [67]. For a comparison of either materials or different radiation sources (particles, energies) the knowledge of the respective dpa would be very valuable. Unfortunately, damage calculations predicting the number of displaced atoms are available only in a few cases. Alternatively, the non-ionizing energy loss was used to show a similar behavior of the change in T_c by irradiation of various cuprate and iron-based superconductors [45].

The influence of the K-concentration in $Ba_{1-x}K_xFe_2As_2$ crystals on the decrease of the transition temperature after neutron irradiation is shown in figure 1. The radiation sensitivity tends to increase with doping level if assessed by the absolute values of T_c. A plausible explanation of a smaller sensitivity of T_c with disorder, as also observed in $LaFe_{1-x-y}Co_xZn_yAsO$, is a weakening of the antiferromagnetism which competes with superconductivity [55]. Indeed, Mizukami *et al* even observed an increase of T_c and a simultaneous decrease of T_N (temperature of antiferromagnetic ordering) following 2.5 MeV electron irradiation in $BaFe_2(As_{1-x}P_x)_2$ with $x = 0.16$ and 0.24 [61]. However, we found the opposite behavior in the phosphorous-doped system, where a significantly higher decrease rate was measured in an under-doped crystal ($BaFe_2(As_{0.76}P_{0.24})_2$) than in the optimally doped system (see table 1). This indicates that either the original or differences in the introduced defect structure have a strong influence in under-doped samples, despite the similar behavior in optimally doped crystals.

By plotting the relative changes (i.e. $\Delta T_c/T_{c0}$) in figure 1, the doping level does not show a significant influence in $Ba_xK_{1-x}Fe_2As_2$ anymore. Note that the reduction in T_c is quite small at this neutron fluence, which strongly amplifies errors of the evaluation. These data obtained from neutron irradiation are in good agreement with findings from Cho *et al* on electron irradiated samples [49, 69]. They also found a fairly smooth behavior of $\Delta T_c/T_{c0}$ near optimal doping (x ranging from 0.26 to 0.34 [49] or from 0.2 to 0.6 [69] with slightly more variation of $\Delta T_c/T_{c0}$), however a strong increase on both the strongly under- and over-doped side. The normalization of ΔT_c by T_{c0} also reduces the difference between the different materials and similar change rates are found for neutron irradiation in the cuprates [10, 62–64] ($(2.6–4.4) \times 10^{-24}\,m^2$) and the iron-based superconductors ($(2.4–6.9) \times 10^{-24}\,m^2$, see table 1) at optimal doping. Bang *et al* [51] indeed predicted a similar rate for the T_c reduction for s_{+-} and *d* wave symmetry when both T_c and the scattering strength are normalized. It is interesting to note that the normalized decrease rate found for Nb_3Sn [13] (about 2×10^{-24} m^2) nearly reaches the lowest values of the unconventional superconductors despite the different underlying mechanism, hence T_c of materials with higher transition temperature tend to be more sensitive to disorder on an absolute scale.

Electrons with an energy of 2.5 MeV introduce much less disorder than neutrons at the same fluence, which is a consequence of their small mass. Hence the decrease in T_c is lower ($\sim 2 \times 10^{-23}$ Km^2) [33, 35, 44] but seem to depend on the pre-existing defect structure with T_c of the cleaner crystal being more sensitive to disorder [35].

3 MeV protons on the other hand reduce the transition temperature significantly faster than neutrons, with a rate between 0.3 and 5.8×10^{-20} Km^2. The enormous spread of data obtained from very similar materials (see table 1) inhibits a comparison of different compounds. It cannot be explained without experimental issues. First, the energy deposition strongly depends on the energy of a charged particle being highest at low energies (a decrease rate of 10^{-18} Km^2 was reported for 200 keV protons), where the Bragg peak occurs (e.g. [67]). Since particles loose energy along their trajectory, the defect density may become very inhomogeneous in

Table 1. Change of T_c resulting from irradiation. The samples are single crystals, unless otherwise indicated. The star * indicates a strongly nonlinear dependence of T_c on fluence.

Compound	Particles	Fluence Φ $\Phi(m^{-2})$	T_{c0} (K)	ΔT_c (K)	$\Delta T_c/\Delta\Phi$ (Km^2)	$\Delta T_c/\Delta\rho$ ($K/\mu\Omega$ cm)
$Ba(Fe_{0.94}Co_{0.06})_2As_2$ [70]	Fast neutrons	3.6×10^{21}	24.2	0.4	10^{-22}	
$Ba(Fe_{0.9}Co_{0.1})_2As_2$ film [37]	200 keV protons	1.8×10^{19}	26	18	10^{-18}	
$Ba(Fe_{1-x}Co_x)_2As_2$ [71]	3 MeV protons	2×10^{20}	21.5	1	5×10^{-21}	
$Ba(Fe_{0.96}Co_{0.04})_2As_2$ [72]	3 MeV protons	1.5×10^{20}	13	0.8	5×10^{-21}	0.02
$Ba(Fe_{0.955}Co_{0.045})_2As_2$ [43]	3 MeV protons	1.2×10^{20}	15.1	2.25	1.9×10^{-20}	0.08
$Ba(Fe_{0.93}Co_{0.07})_2As_2$ [73]	3 MeV protons	1.2×10^{20}	~24	~3	$\sim 2.5 \times 10^{-20}$	
$Ba(Fe_{0.93}Co_{0.07})_2As_2$ [18]	3 MeV protons	1.2×10^{20}	24.8	1.5	1.25×10^{-20}	0.13
$Ba(Fe_{0.925}Co_{0.075})_2As_2$ [24]	3 MeV protons	2×10^{20}	24.4	2	10^{-20}	
$Ba(Fe_{0.925}Co_{0.075})_2As_2$ [43]	3 MeV protons	1.2×10^{20}	24.8	7	5.8×10^{-20}	0.2
$Ba(Fe_{0.887}Co_{0.113})_2As_2$ [43]	3 MeV protons	1.2×10^{20}	12.8	1.5	1.25×10^{-20}	0.13
$Ba(Fe_{0.93}Co_{0.07})_2As_2$ [17]	200 MeV Au	10^{15}	24	0	0	
$Ba(Fe_{0.93}Co_{0.07})_2As_2$ [18]	200 MeV Au	7.7×10^{15}	24.4	4.6	$6 \times 10^{-16*}$	
$Ba(Fe_{0.93}Co_{0.07})_2As_2$ [18]	800 MeV Xe	5.3×10^{15}	24.4	1.8	3.4×10^{-16}	
$Ba(Fe_{0.92}Co_{0.08})_2As_2$ [74]	1.4 GeV Pb	1.7×10^{15}	26	1	6×10^{-16}	
$Ba(Fe_{0.93}Co_{0.07})_2As_2$ [18]	2.6 GeV U	7.7×10^{15}	24.4	2.4	3×10^{-16}	
$Ba(Fe_{0.925}Co_{0.075})_2As_2$ [75]	2.6 GeV U	$1/8 \times 10^{15}$	24.4		$1.25/0.18 \times 10^{-15}$	
$Ba(Fe_{0.76}Ru_{0.24})_2As_2$ [44]	2.5 MeV electrons	2.1×10^{23}	17.8	4.3	2×10^{-23}	0.35
$BaFe_2(As_{0.76}P_{0.24})_2$	Fast neutrons	1.8×10^{21}	16	1	5.5×10^{-22}	
$BaFe_2(As_{0.7}P_{0.3})_2$ [70]	Fast neutrons	3.6×10^{21}	29.1	0.7	2×10^{-22}	
$BaFe_2(As_{0.72}P_{0.28})_2$ [61]	2.5 MeV electrons	1.1×10^{23}	30	2	1.8×10^{-23}	0.28
$BaFe_2(As_{0.71}P_{0.29})_2$ [61]	2.5 MeV electrons	1.3×10^{23}	30.3	2.1	1.6×10^{-23}	0.25
$BaFe_2(As_{0.7}P_{0.3})_2$ [61]	2.5 MeV electrons	1.4×10^{23}	31.7	3.4	2.4×10^{-23}	0.31
$BaFe_2(As_{0.65}P_{0.35})_2$ [33]	2.5 MeV electrons	2.8×10^{23}	30	5.7	2×10^{-23}	0.3
$SrFe_2(As_{0.65}P_{0.35})_2$ [35]	2.5 MeV electrons	1.4×10^{23}	34.7	5.7	4×10^{-23}	
$SrFe_2(As_{0.65}P_{0.35})_2$ [35]	2.5 MeV electrons	7×10^{22}	32.5	1.5	2.1×10^{-23}	
$Ba_{0.77}K_{0.23}Fe_2As_2$ [68]	Fast neutrons	1.7×10^{21}	23.1	0.1	6×10^{-23}	
$Ba_{0.6}K_{0.4}Fe_2As_2$ [70]	Fast neutrons	3.6×10^{21}	38.4	0.6	1.7×10^{-22}	
$Ba_{0.81}K_{0.19}Fe_2As_2$ [49]	2.5 MeV electrons	1.1×10^{23}	14	4.8	4.4×10^{-23}	0.11
$Ba_{0.74}K_{0.26}Fe_2As_2$ [49]	2.5 MeV electrons	9.4×10^{22}	32	3.1	3.3×10^{-23}	0.2
$Ba_{0.66}K_{0.34}Fe_2As_2$ [49]	2.5 MeV electrons	1.2×10^{23}	38	4.2	3.4×10^{-23}	0.19
$Ba_{0.4}K_{0.6}Fe_2As_2$ [69]	2.5 MeV electrons	1.1×10^{23}	29.3	2	1.8×10^{-23}	0.13
$Ba_{0.32}K_{0.68}Fe_2As_2$ [69]	2.5 MeV electrons	1.1×10^{23}	20.7	1.9	1.7×10^{-23}	0.1
$Ba_{0.22}K_{0.78}Fe_2As_2$ [69]	2.5 MeV electrons	1.1×10^{23}	16.4	2.1	1.9×10^{-23}	0.08
$Ba_{0.19}K_{0.81}Fe_2As_2$ [69]	2.5 MeV electrons	1.1×10^{23}	10.2	2.8	2.5×10^{-23}	0.11
$Ba_{0.08}K_{0.92}Fe_2As_2$ [69]	2.5 MeV electrons	7.5×10^{22}	6.7	1.7	2.2×10^{-23}	0.1
KFe_2As_2 [69]	2.5 MeV electrons	7.5×10^{22}	4	2.2	3×10^{-23}	0.08
$Ba_{0.77}K_{0.23}Fe_2As_2$ [36]	3 MeV protons	9.2×10^{20}	24.4	4.3	4.7×10^{-21}	0.065
$Ba_{0.31}K_{0.69}Fe_2As_2$ [36]	3 MeV protons	9.2×10^{20}	17.8	4.3	4.7×10^{-21}	0.161
$Ba_{0.58}K_{0.42}Fe_2As_2$ [36]	3 MeV protons	9.2×10^{20}	37.4	3	3.3×10^{-21}	0.095
$Ba_{0.6}K_{0.4}Fe_2As_2$ [76]	3 MeV protons	5.8×10^{20}	38.6	3.5	6×10^{-21}	
$Ba_{0.6}K_{0.4}Fe_2As_2$ [58]	4 MeV protons	7×10^{20}	38.3	1	1.4×10^{-21}	
$Ba_{0.6}K_{0.4}Fe_2As_2$ [19]	1.4 GeV Pb	2.4×10^{16}	37.5	2	8×10^{-17} *	
$Ba_{0.6}K_{0.4}Fe_2As_2$ [34]	1.4 GeV Pb	1.9×10^{15}	39	0	0	
$Ca_{0.5}Na_{0.5}Fe_2As_2$ [42]	3 MeV protons	2×10^{20}	19.4	1.6	8×10^{-21}	0.053
$Ca_{0.85}La_{0.15}Fe_2(As_{0.92}Sb_{0.08})_2$ [77]	3 MeV protons	10^{20}	34	3	3×10^{-20}	
$Ca_{8.5}La_{1.5}(Pt_3As_8)(Fe_2As_2)_5$ [78]	Protons	5×10^{19}	32.5	2.2	4.4×10^{-20}	0.0046
$NdFeAsO_{1-x}F_x$ [79]	Fast neutrons	3.7×10^{21}	39.9	0.6	1.6×10^{-22}	
$SmFeAsO_{0.65}F_{0.35}$ [8] (poly)	Fast neutrons	1.1×10^{22}	53.6	1.7	1.5×10^{-22}	0.017
$LaFeAsO_{0.9}F_{0.1}$ [41] (poly)	Fast neutrons	1.6×10^{23}	30.5	30.5	$>1.9 \times 10^{-22}$	
$NdFeAsO_{0.7}F_{0.3}$ [80]	2 MeV He	3×10^{19}	46.4	6.4	1.5×10^{-22}	0.04
$FeSe_{0.5}Te_{0.5}$ [81] (film)	Fast neutrons	1.2×10^{21}	19.35	0.3	2.5×10^{-22}	
$FeSe_{0.5}Te_{0.5}$ [60]	Fast neutrons	1.8×10^{21}	14.4	0	0	
$FeSe_{0.3}Te_{0.7}$ [60]	Fast neutrons	1.8×10^{21}	14.2	−0.15	-8×10^{-23}	
$FeSe_{0.5}Te_{0.5}$ [59] (film)	190 keV protons	1×10^{19}	18.0	−0.5	-5×10^{-20}	
FeSe [22]	2.5 MeV electrons	1.1×10^{23}	8.8	−0.4	-3.6×10^{-24}	

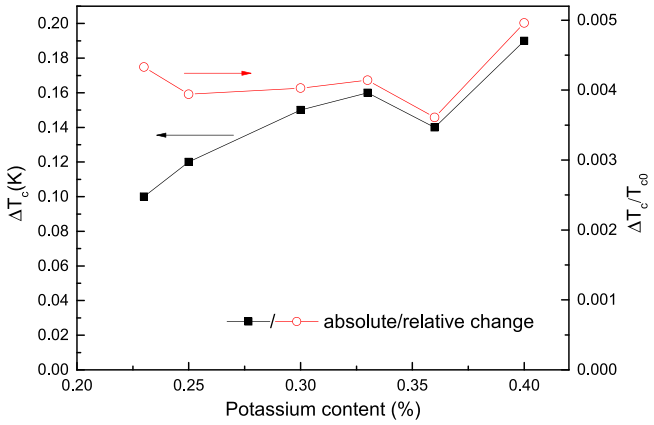

Figure 1. Decrease of the transition temperature after neutron irradiation to a fast neutron fluence of 1.7×10^{-21} m^{-2} as a function of the doping level x in $Ba_{1-x}K_xFe_2As_2$ [68]. T_{c0} refers to the transition temperature before irradiation.

thicker samples. Another important parameter is the temperature during the irradiation process. *In situ* defect annealing (e.g. recombination of Frenkel pairs) increases with temperature, local melting and/or phase decomposition on the other hand is favored by high temperatures. The influence of the doping level on the change in T_c is also not obvious from the proton irradiation experiments. While the largest decrease of T_c was reported at optimal doping in the Co-doped system [43], the opposite was found in K-doped samples [36]. The latter contrasts the findings from neutron irradiation experiments (figure 1).

The highest damage per particle is introduced by high energy heavy ions. It is however concentrated along the ion's trajectory mainly forming extended defects. At low fluences, the superconducting matrix between these defects remains nearly undisturbed and the influence on the transition temperature is small [17, 18, 34]. At high fluences, the large dpa number leads to a fast decrease of T_c with a rate of $(3–6) \times 10^{-16}$ Km^2 in Co- and P-doped Ba-122, while significantly smaller values were reported for the K-doped system [19, 34].

Since the decrease in T_c is most likely caused by scattering of the charge carriers, the decrease rate with respect to the change in resistivity (typically close to T_c) is inherently more meaningful than its dependence on fluence. It is also favorable for the comparison between different compounds and irradiation techniques. Available literature data are summarized in the last column of table 1. Unfortunately, they do not reveal unambiguous trends, although the highest values of $\Delta T_c/\Delta\rho$ are reported after electron irradiation [33, 44, 61]. Unfortunately, resistivity data referring to irradiation experiments with other particles are scarce. Comparable data for the K-doped Ba-122 after proton irradiation indicate a smaller $T_c/\Delta\rho$. The lowest value for Ba-122 on the other hand refers to an under-doped sample [72], which can be considered, together with the fluence dependence of T_c shown in figure 1, as evidence for a higher radiation tolerance of under-doped materials having a lower T_c. However, comprehensive electron irradiation studies on $Ba_xK_{1-x}Fe_2As_2$ [49, 69] clearly indicate that the decrease of the normalized T_c with resistivity is smallest near optimal doping and increase systematically with over- or under-doping.

The $FeSe_xTe_{1-x}$ compound shows a different behavior and an increase of the transition temperature was found after neutron [60], proton [59], and electron [22] irradiation. This remarkable result highlights a mechanism for an increase in transition temperature which can overcompensate the detrimental effect of disorder on T_c. Ozaki *et al* explained their findings by nanoscale lattice strain [59], which locally increases T_c in compressed areas (this effect was demonstrated by Bellingeri *et al* [82]) either forming a percolative network or linked via the proximity effect. Teknowijoyo *et al* [22] on the other hand proposed pair-strengthening by Frenkel pairs, which locally enhance magnetic fluctuations, to be responsible for the enhanced T_c [22]. Weakening of long-range antiferromagnetic ordering, as proposed to cause the increase of T_c in under-doped Ba-122 [61], can be ruled for $FeSe_xTe_{1-x}$.

3.3. Upper critical field

A reduction in mean free path of the charge carriers leads to an increase of the upper critical fields in isotropic *s*-wave superconductors; thus, scattering induced by the defects resulting from irradiation should increase the upper critical field. This was demonstrated in Nb_3Sn [83] and more spectacularly in MgB_2, where B_{c2} can increase by a factor of three or more due to the introduction of efficient scattering centers [84, 85]. The mean free path of the charge carriers has to be similar or smaller (dirty limit) than the clean limit coherence length for a significant (relative) change of B_{c2}. Since the Ginzburg–Landau coherence length ξ is only around 2 nm in most iron-based superconductors (see table 2), an even smaller value of the mean free path seems incompatible with the pair-breaking effects of non-magnetic impurities in these materials and one can expect only a weak effect on the upper critical field. Indeed, only small changes in upper critical fields were observed after irradiation [8, 32, 42, 71, 81, 86] and the positive effect of an increase in scattering (larger slope of dB_{c2}/dT near T_c) has to compete with the accompanying decrease of the transition temperature. The anisotropy of B_{c2} is reduced [19, 42, 81, 86], with the strongest effect being reported for Sm-1111 after irradiation with 1.4 GeV Pb ions [87]. This agrees with the general trend that scattering makes the material more homogeneous. The decrease in anisotropy impedes a further enhancement of B_{c2} for $H\|ab$, but fosters an improvement for $H\|c$.

3.4. Magnetic penetration depth and superfluid density

For thermodynamic reasons, the magnetic penetration depth, λ, is directly connected to changes in ξ. The Ginzburg–Landau relation $B_c = \frac{\phi_0}{2\sqrt{2}\pi\lambda\xi}$ implies that they change inversely if the thermodynamic critical field, B_c, does not change. Since T_c and B_c both scale with the superconducting gap, Δ, this can be checked easily from the change in transition

temperature. If T_c and B_{c2} (ξ) do not change significantly, this should also hold for λ. However, a strong increase of λ from 260 to 430 nm was reported in $Ca_{0.5}Na_{0.5}Fe_2As_2$ due to irradiation with 3 MeV protons [42]. This strong change together with a weak effect on B_{c2} and T_c (−2 K) is obviously inconsistent with this picture and the authors explained it with a breakdown of Abrikosov–Gorkov theory. Multi-band effects may play a role as well.

4. Critical currents

Irradiation techniques are a very efficient way of changing the defect landscape in superconducting materials to investigate the resulting change of the flux pinning behavior and the critical current densities. Nearly all data in this section were obtained by magnetization measurements, where the magnetic field was applied parallel to the crystallographic *c*-direction, thus the shielding currents flow parallel to the FeAs (or FeSe) layers. The latter is also ensured for the few data obtained on thin films. We assume that the critical current density is isotropic within these planes and denote the in-plane critical current density as J_c. First, the neutron irradiation studies on iron-based superconductors conducted at TU Wien will be summarized. Afterwards, they will be compared to the literature for other radiation techniques.

Figure 2 presents the field dependence of J_c in different compounds at various temperatures and its change after neutron irradiation. The open and solid symbols refer to the pristine and irradiated crystals, respectively. The same color code and the same symbols are used for the same temperature in all the panels. While the Co-, P-, and K-doped Ba-122 crystals are close to optimal doping in view of their high transition temperature, the Nd-1111 crystal is under-doped as indicated by its low T_c (39.3 K).

The field dependence of the critical current density is non-monotonic in the pristine Co- and P- doped Ba-122 and the Nd-1111 crystals ('fishtail' or 'second peak' effect), J_c is in addition non-monotonic in temperature at certain fields in the phosphorus doped sample (top right panel in figure 2). This behavior is likely caused by an order-disorder transition of the flux line lattice, where flux pinning transforms the ordered flux line lattice into a glassy state [88, 89]. This leads to a better adaption of the vortices to the defect structure resulting in higher critical current densities. After neutron irradiation, the added defects increase the overall pinning energy significantly resulting in a disordered vortex lattice at all fields and temperatures; the fishtail disappears. If a second peak effect is observed in the pristine sample, the currents are enhanced the most at low fields near the position of the local minima in $J_c(B)$ of the unirradiated material (originally 'ordered' vortex state) and the changes are small near the irreversibility field ('disordered' vortex state already in the unirradiated crystal). If pinning is very weak (K-doped crystal) and the vortex lattice remains fairly ordered at all fields before the irradiation, the enhancement is generally larger (transition to a disordered flux line lattice), in particular at high fields. This overall behavior of J_c in iron-based single crystals is very similar to that in the cuprate superconductors [63, 90, 91].

It is interesting to note that J_c below 15 K is higher in the pristine Co-doped sample (top left panel in figure 2) than in the P-(top right panel) or K-doped crystal (bottom left panel). (At higher temperatures, the influence of the transition temperature becomes dominant.) After the irradiation, J_c becomes highest in the K-doped Ba-122 crystal at all fields and temperatures, the order of J_c in these three crystals is thus reversed. In particular at high temperatures, the J_c increase in the K-doped crystal is spectacular (many orders of magnitude), however without a significant shift of the irreversibility line [70]. The differences in the pristine materials result presumably from the different position of the dopant atoms. Cobalt replaces iron, whose orbitals provide the charge carriers, thus being a much stronger scatterer (and a more efficient pinning center) than the phosphorus atoms which replace the arsenic atoms. Potassium substitutes the barium atoms in between the FeAs layer which are responsible for superconductivity, the defect structure in the pristine crystal pins vortices only very weakly. After introducing a more efficient pinning structure by the irradiation, which can be considered as identical in all systems, the fundamental superconducting properties (magnetic penetration depth, λ, and coherence length, ξ) have to be responsible for any differences, as will be discussed below.

The currents in the Nd-1111 crystal (bottom rigth panel in figure 2) are of the same order of magnitude as in the Co- and P-doped 122 crystals and the increase in J_c after irradiation is similar.

The right panel in figure 3 highlights that the critical current densities in an under-doped Ba-122 sample (24% P, $T_c = 16$ K) are smaller by more than one order of magnitude than in the optimally phosphorous-doped crystal ($T_c = 29.4$ K). No fishtail effect occurs and the magnetic field rapidly suppresses the critical currents. The increase in J_c after irradiation is much smaller, thus the difference between under-doped and optimally doped crystal even grows with the introduction of the defects. Weak pinning can thus be ruled out as the reason for the low J_c in the under-doped sample.

Rather small critical current densities are also observed in the 11 crystal ($T_c = 15$ K, figure 3, left panel), although they do not decrease with magnetic field as strongly as in the under-doped 122 crystal. The irradiation increases J_c also in this case, it remains however modest, which can be partly related to the small depairing current density in this compound (see below).

Figure 4 compares the temperature dependence of J_c in the crystals under consideration. In the pristine state (open symbols) at 1 T (left top panel) and low temperatures, the behavior is similar (J_c within a factor of two) in the 1111 (brown stars) and the optimally doped 122 (green and red triangles, black squares) crystals. The same is true for the 11 (blue circles) and the under-doped 122 (cyan diamonds) crystal, but their J_c is considerably smaller and its temperature dependence at low temperatures is stronger.

In order to eliminate the effect of the different transition temperatures the same data are re-plotted as a function of the reduced temperature in the lower panels. The slopes in

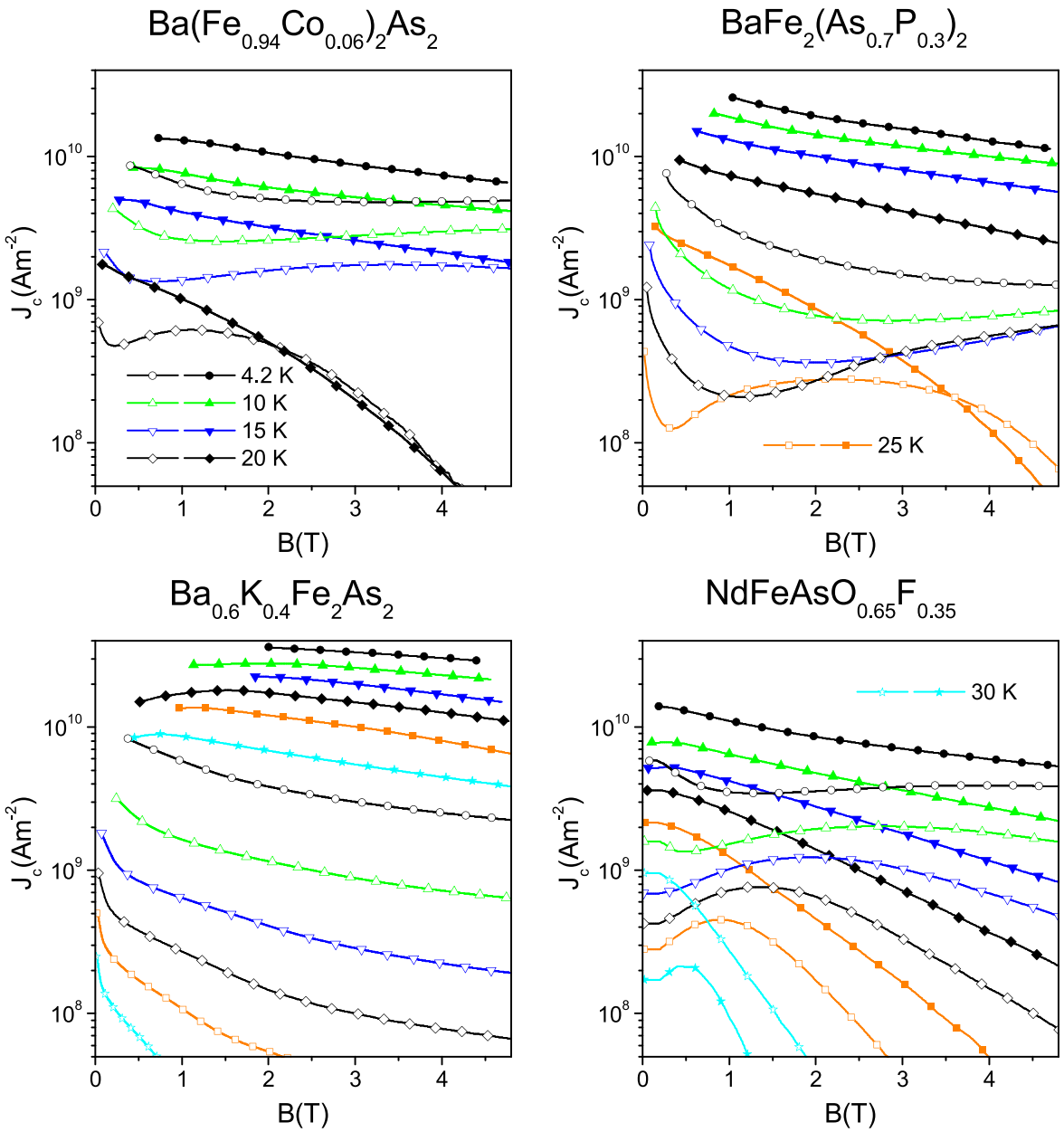

Figure 2. Critical current density in $Ba(Fe_{0.94}Co_{0.06})_2As_2$, $BaFe_2(As_{0.7}P_{0.3})_2$, and $K_{0.4}Ba_{0.6}Fe_2As_2$ crystals. Open and solid symbols refer to the pristine and irradiated (1.8×10^{21} m^{-2}) samples, respectively. The neutron fluence for the Nd-1111 crystal was 3.7×10^{21} m^{-2}. The same symbols always refer to the same temperature in all panels.

Table 2. Magnetic penetration depth, coherence length, depairing current density, Ginzburg number and pinning efficiency after neutron irradiation to the given fluence.

Compound	ξ (nm)	λ (nm)	J_d (10^{10} Am^{-2})	G_i	η (%)	$\phi_n t$ (10^{21} m^{-2})
$Ba(Fe_{0.94}Co_{0.06})_2As_2$ [92–97]	2.35	240	74	2.5×10^{-4}	2.3	3.6
$BaFe_2(As_{0.7}P_{0.3})_2$ [97–99]	2.7	182	110	9×10^{-5}	2.4	3.6
$Ba_{0.6}K_{0.4}Fe_2As_2$ [97, 100, 101]	1.5	200	170	8×10^{-4}	3.4	3.6
$NdFeAsO_{1-x}F_x$ [102–105]	1.5	200	170	3.5×10^{-2}	0.8	3.7
$FeSe_{0.5}Te_{0.5}$ [2, 106–108]	1.2	560	26	5×10^{-3}	0.32	1.8

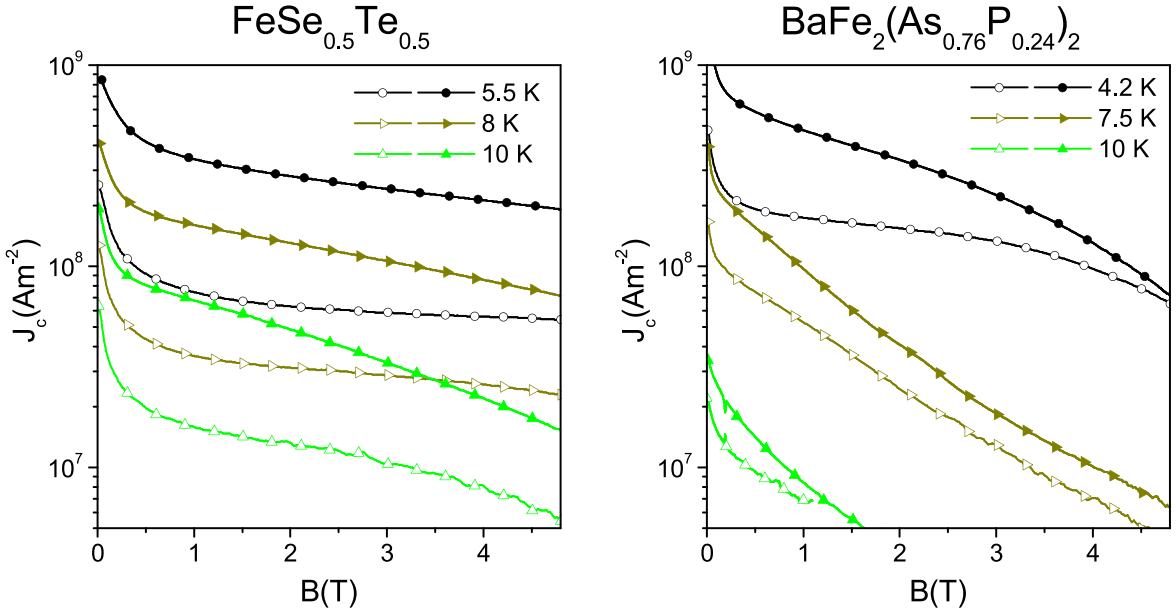

Figure 3. Critical current density in $FeSe_{0.5}Te_{0.5}$ ($T_c = 15$ K) and $BaFe_2(As_{0.76}P_{0.24})_2$ ($T_c = 16$ K) and the influence of neutron irradiation (1.8×10^{21} m^{-2}).

the pristine optimally doped Ba-122 crystals are now anti-correlated with the absolute values. The highest currents with the smallest temperature dependence are observed for the Co-doped crystal, the lowest currents with the largest slope are found in the K-doped system. This is consistent with the largest pinning potential, which can compete best with the thermal energy, resulting from the cobalt atoms. The pinning potential resulting from the K-atoms is weakest, but their density is largest, which may explain the cross-over of the $J_c(t)$ curves of the K- and P-doped crystals. At low temperatures, a higher density of pins can outweigh a smaller pinning energy per defect. At higher fields (4 T, right panels), the data become more heterogeneous, in particular the temperature dependence of the 1111 crystal (at low temperatures) becomes stronger than in the Co- or P-doped 122 crystals, the latter showing the flattest $J_c(t)$ behavior of all crystals.

The irradiation has the largest effect in the K-doped crystal and its J_c becomes the highest of all crystals at all fields and temperatures. Note that the enhancement rather reflects the weakness of pinning in the pristine state than the efficiency of the radiation induced defects. However, a strong increase of J_c ensures that the introduced defects dominate the pinning properties allowing the assumption that the pinning effective defect structure is nearly the same in all compounds after the irradiation. Differences result in this case predominantly from the intrinsic material properties. The following discussion refers to J_c of irradiated samples (solid symbols in the figures) under the assumption that the radiation induced defect structure is relevant for the observed currents.

From the magnetic penetration depth and the superconducting coherence length, the depairing current density

$$J_d = \frac{\phi_0}{3\sqrt{3}\,\pi\mu_0\lambda^2\xi} \tag{1}$$

and the Ginzburg number

$$G_i = \frac{1}{2}\left(\frac{2\pi\mu_0 k_B \gamma\lambda^2(0)T_c}{\phi_0^2\xi(0)}\right)^2 \tag{2}$$

can be calculated. Table 2 lists λ and ξ for the different compounds taken from literature and the calculated J_d and G_i. These values can be considered as rough estimates only, because the literature data strongly scatter and in some cases refer to samples of slightly different composition (doping level).

The depairing current density J_d sets the magnitude of achievable currents, although it cannot be reached under conditions relevant for applications, because flux pinning rather than depairing limits the achievable currents when vortices enter the superconductor. The self field of the currents is sufficient to generate vortices, unless at least one sample dimension is extremely small.

The largest pinning force can be obtained if the entire core energy per unit length, $E_{core} = \frac{\phi_0^2}{16\pi\mu_0\lambda^2}$, is gained along a (linear or planar) defect. Since the condensation energy changes on the length scale of ξ, the resulting force per length is approximately $f_p \sim E_{core}/\xi$. Balancing the pinning force acting on one vortex with the Lorentz force per unit length, $\iint F_L = \iint J_c B = J_c\phi_0$, defines a maximally achievable critical current density $J_c^{max} = f_p/\phi_0 = 3\sqrt{3}/16 J_d = \eta_{max} J_d \approx 0.32 J_d$. The current was assumed to flow perpendicular to the vortex and the integration of the field of a single vortex over the entire

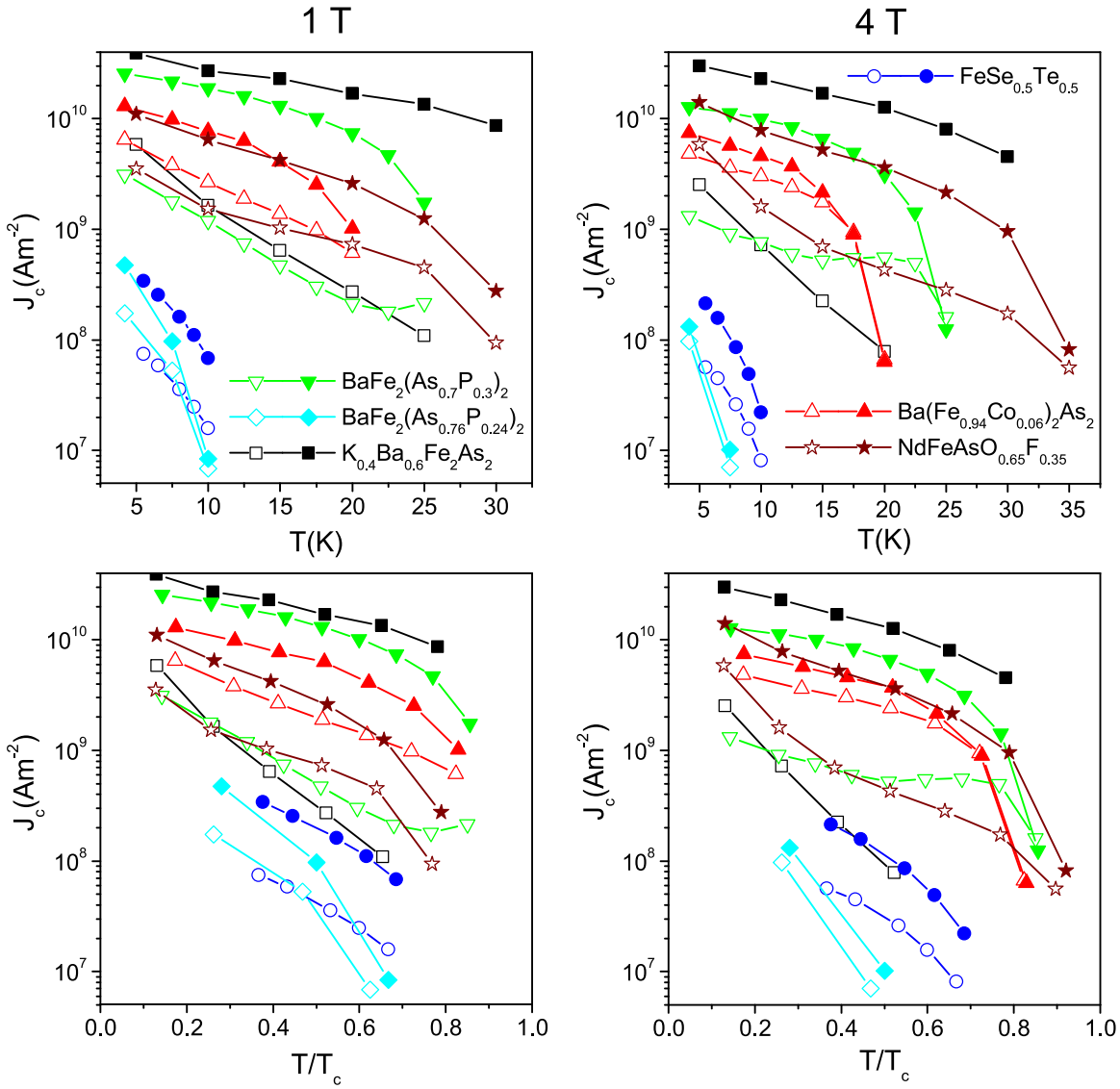

Figure 4. Temperature dependence of the critical currents (top panels) at 1 T (left) and 4 T(right). Bottom panels: same data but with the temperature normalized to T_c.

perpendicular plane results in the elementary flux quantum ϕ_0. The pinning efficiency, η, is defined by the ratio between J_c and J_d. Its maximum value, η_{max}, is universal since all material properties influence J_d only. In real conductors, however, one can obtain typically 10%–20% of the depairing current density of the respective compound by optimizing pinning (linear defects which pin the flux line along its whole length). Since the defect cascades, which result from fast neutron irradiation, are spherical defects with a radius of 2–3 nm, they only interact along short segments of the vortices and the critical currents are accordingly smaller. For example, the self-field critical current density reaches about 2%–3% of J_d at low temperatures in single crystals of the cuprates. In order to compare the efficiency of the pinning structure following neutron irradiation in the iron-based compounds, the self-field J_c at low temperature (i.e. 4.2–5.5 K) was divided by the depairing current density. The corresponding values $\eta = J_c/J_d$ are listed in table 2.

The pinning efficiencies in the irradiated Ba-122 crystals are in good agreement with each other and the findings in cuprates. This confirms that the similar defect structure resulting from neutron irradiation in these compounds leads to a similar pinning efficiency and the different critical current densities are mainly resulting from the varying depairing current density. The pinning efficiency in the K-doped crystal is the highest, but given the large uncertainties for λ, the interpretation is not reliable at present. The low values in the 1111 crystal are likely caused by an overestimated J_d, since λ and ξ were obtained from measurements on crystals with a significantly higher T_c. The depairing current density is likely much smaller in our under-doped (low T_c) crystal. The very low η in the 11 crystal on the other hand is certainly influenced by the comparatively high reduced temperature $t = T/T_c = 5.5/15 \approx 0.37$ it refers to. From the temperature dependence of J_c presented in figure 4 one can extrapolate an increase in J_c by around a factor of 3 when the reduced temperature is decreased to about 0.14 (reduced temperature the other data refer to). However, even in that case η would remain significantly lower than in the other materials, which

Table 3. Overview of self-field critical current densities and the resulting pinning efficiency in irradiated sampes at low temperatures (2–5.5 K).

Compound	Particles	J_c (MA cm^{-2})	η (%)
$Ba(Fe_{0.94}Co_{0.06})_2As_2$ [70]	Fast neutrons	1.7	2.3
$Ba(Fe_{0.96}Co_{0.04})_2As_2$ [72]	3 MeV protons	0.08	
$Ba(Fe_{0.93}Co_{0.07})_2As_2$ [73]	3 MeV protons	2	2.7
$Ba(Fe_{0.93}Co_{0.07})_2As_2$ [18]	3 MeV protons	1.8	2.4
$Ba(Fe_{0.925}Co_{0.075})_2As_2$ [24]	3 MeV protons	1.8	2.4
$Ba(Fe_{0.93}Co_{0.07})_2As_2$ [18]	200 MeV Au	4	5.4
$Ba(Fe_{0.93}Co_{0.07})_2As_2$ [18]	800 MeV Xe	2	2.7
$Ba(Fe_{0.92}Co_{0.08})_2As_2$ [74]	1.4 GeV Pb	2.1	2.8
$Ba(Fe_{0.93}Co_{0.07})_2As_2$ [18]	2.6 GeV U	3	4
$Ba(Fe_{0.925}Co_{0.075})_2As_2$ [75]	2.6 GeV U	3	4
$Ba(Fe_{0.925}Co_{0.075})_2As_2$ [109]	1.4 GeV Pb	0.95	1.3
$BaFe_2(As_{0.76}P_{0.24})_2$	Fast neutrons	0.05	
$BaFe_2(As_{0.7}P_{0.3})_2$ [70]	Fast neutrons	2.6	2.4
$Ba_{0.6}K_{0.4}Fe_2As_2$ [70]	Fast neutrons	7	4.1
$Ba_{0.6}K_{0.4}Fe_2As_2$ [76]	3 MeV protons	11	6.5
$Ba_{0.6}K_{0.4}Fe_2As_2$ [58]	4 MeV protons	6.2	3.6
$Ba_{0.6}K_{0.4}Fe_2As_2$ [19]	1.4 GeV Pb	5	2.9
$Ca_{0.85}La_{0.15}Fe_2(As_{0.92}Sb_{0.08})_2$ [77]	3 MeV protons	4.5	
$NdFeAsO_{1-x}F_x$ [79]	Fast neutrons	1.4	0.8
$SmFeAsO_{0.8}F_{0.15}$ [87]	1.4 GeV Pb	20	11.8
$FeSe_{0.5}Te_{0.5}$ [81] (film)	Fast neutrons	0.5	1.9
$FeSe_{0.5}Te_{0.5}$ [70]	Fast neutrons	0.08	0.3
$FeSe_{0.3}Te_{0.7}$ [70]	Fast neutrons	0.04	0.15
$FeSe_{0.5}Te_{0.5}$ [59] (film)	190 keV protons	1.4	5.4
$FeSe_{0.39}Te_{0.71}$ [18]	200 MeV Au	0.5	1.9

cannot be solely explained by the lower neutron fluence. Further efforts are necessary to clarify the small critical current density in this 11 crystals as well as in the under-doped Ba-122 crystal.

Table 3 summarizes critical current densities achieved by various irradiation techniques. The results after proton or neutron irradiation are quite similar although J_c is slightly higher for protons and obtained at a smaller fluence, both of these effects are also observed in Nb_3Sn [14, 66, 67]. The only exception is the 11 compound, where low energy (190 keV) protons [59] lead to significantly higher currents than neutrons. It has to be clarified whether this is related to the material, or a consequence of the low proton energy.

The self field J_c in Ba-122 after heavy ion irradiation with 1.4 GeV Pb or 800 MeV Xe is also comparable to results from protons or neutrons, higher values were achieved with 2.6 GeV U and 200 MeV Au [17] ions. In Sm-1111 on the other hand, 1.4 GeV Pb ions induced a record J_c with the highest pinning efficiency reported so far [87]. However, the main difference in pinning resulting from different irradiation techniques manifests itself in the field dependence of J_c. The linear defects introduced by heavy ion irradiation can cause a very weak field dependence of J_c below the matching field, B_m, where the density of the vortices becomes equal to the defect density. If every vortex is pinned by a columnar defect, the single vortex pinning limit used above for the derivation of the maximally possible pinning efficiency persists and the critical current becomes independent of the field in the ideal case. In fact, a very small field dependence of J_c was observed at low fields in Co-doped Ba-122 crystals after irradiation with 1.4 GeV Pb ions [19, 58, 74], which contrasts the behavior of the three-dimensional defects caused by neutrons or protons. In the latter case, a power-law $J_c \propto B^{-\alpha}$ with α around 0.5 is often observed [24, 58, 70, 73]. Interestingly, adding proton induced defects to the linear defects can extend the field range with nearly field independent J_c and shifts the onset of the power-law behavior closer to B_m [58]. This was ascribed to the suppression of kink formation of the vortices which enables hopping from one pinning center to the other, hence reducing J_c already well below B_m. This depinning mechanism is likely responsible for the absence of a low field region with a nearly constant current density in Sm-1111 [87] after 1.4 GeV Pb irradiation, since thermal fluctuations are more important in this compound due to its significantly larger Ginzburg number (see table 2).

A confirmation that the radiation induced defect structure dominates the pinning behavior in Ba-122 was given by an analysis of the field dependence of the volume pinning force [70]. Despite large differences in the pristine state, the differently doped (Co, P, K) crystals behaved identically after neutron irradiation. The position of the maximum in the pinning force was found at a reduced field ($b = B/B_{irr}$ with B_{irr} being the field where the critical current becomes zero) of about 0.2, which points towards dominant pinning by large, diluted defects. A similar analysis with a P-doped proton irradiated crystal revealed the maximum of the pinning force

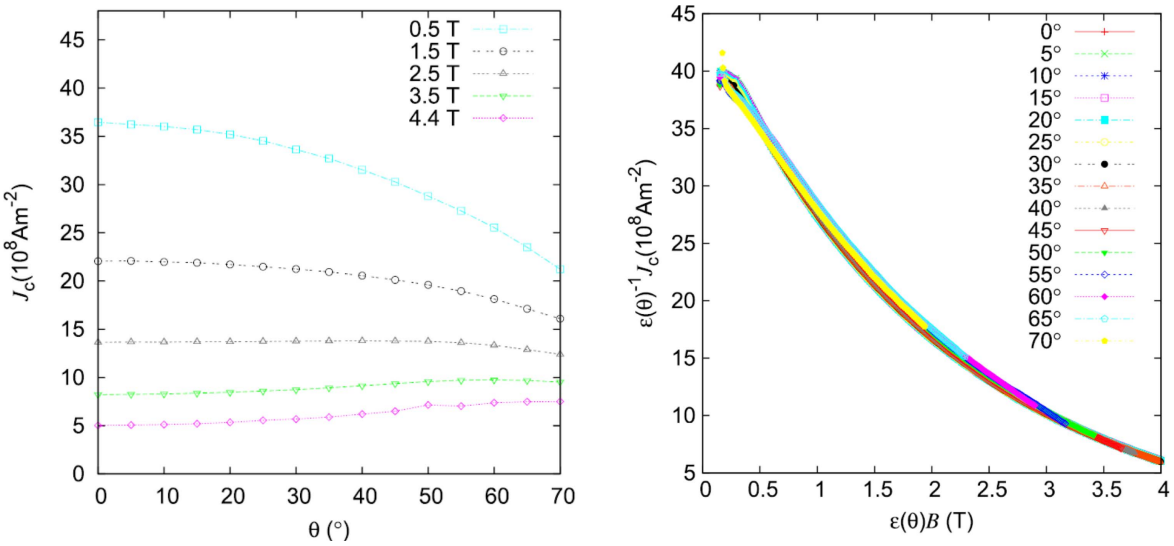

Figure 5. Anisotropy of the critical current density in a neutron irradiated Co-doped Ba-122 crystal. Left panel: angular dependence of J_c at 17.5 K. Right panel: scaling of $J_c(B)$ at various angles. Reproduced from [111].© IOP Publishing Ltd. CC BY 3.0.

at $b = 0.35$ in a strongly over-doped sample [110]. This difference indicates the transition from δT_c-pinning in the optimal doped crystal to δl-pinning as the coherence length becomes larger than the radiation induced defects in the over-doped system.

Very few data are available for the angular dependence of J_c in irradiated iron-based superconductors. Defects resulting from proton or neutron irradiation are isotropic and perfectly suited to investigate the isolated influence of the electronic mass anisotropy on $J_c(\theta)$. A powerful tool for the prediction of anisotropy effects was proposed by Blatter *et al* [112]. The idea is to scale parameters such as field or temperature with fuctions of $\epsilon(\theta) = \sqrt{\gamma^{-2}\sin^2(\theta) + \cos^2(\theta)}$, where γ is the anisotropy of the upper critical field $\gamma = B_{c2}^{ab}/B_{c2}^{c}$. In the single vortex pinning regime of collective pinning theory, the angular dependence of J_c can then be simply described by $J_c(B, \theta) = J_c(B\epsilon(\theta), \theta = 0)$. Hence, knowing J_c for $H\|c$ and γ is sufficient for a description of the entire angular range. Mishev *et al* [111] demonstrated the validity of this approach with a K-doped Ba-122 crystal, which showed very weak pinning (see left bottom panel in figure 2). Data obtained on an irradiated Co-doped crystal on the other hand could not be described in this way. Instead, the current had to be scaled as well, resulting in the scaling law $J_c(B, \theta) = \epsilon(\theta)J_c(B\epsilon(\theta), \theta = 0)$. This scaling law is demonstrated in the right panel of figure 5. The authors related this behavior to the radius of the defects, being smaller than the coherence length in the weak pinning case but larger after the irradiation. The salient point is a qualitative reversal of the J_c-anisotropy at low fields. While the small defects lead to a maximum in $J_c(\theta)$ for $H\|ab$, large defects do so for $H\|c$ (e.g. 0.5 T data in the left panel of figure 5). The influence of field scaling dominates at high fields leading to a peak at $H\|ab$ in any case (e.g. curve for 4.4 T). At intermediate fields, the maximum can even occur in between the two main field orientations [111].

Maiorov *et al* [71] assessed the angular dependence of J_c in a Co-doped film prior to and following proton irradiation. The film contained c-axis correlated defects leading to a large peak in $J_c(\theta)$ for $H\|c$. The proton irradiation was much more beneficial near $H\|ab$ than in the perpendicular orientation. Note that these experiments were done at much lower temperature (hence in the low field limit), but the results seem opposite to the findings from neutron irradiation, although a peak at intermediate angles was observed as well. However, the interplay between two types of strong defects is always complex and can lead to additional effects, as demonstrated by the combined irradiation with heavy ions and protons [58] where the proton induced defects extended the low field plateau of the 1.4 GeV Pb ion irradiated crystal. In contrast, the pure defect structure arising from proton irradiation does not lead to a low field plateau at all (except self-field effects).

The influence of radiation on flux creep is generally beneficial: the pinning barrier increases, the creep rate is reduced [17, 18, 73–76]. This was demonstrated by heavy ion [17, 18, 74, 75] and proton [18, 73, 76, 113] irradiation, in Co-[17, 18, 73–75] and K-[76] doped Ba-122 as well as in FeSe [113]. The defects introduced by neutron, proton or ion irradiation are hence larger than the typical defects that are naturally present in crystals.

5. Conclusions

Irradiation results on iron-based superconductors were reviewed and compared to similar experiments on other materials. Changes in the fundamental material properties, such as gap symmetry and transition temperature, by impurity scattering were assessed in many studies but their interpretation is complicated by the multi-band (super)conductivity of the iron-based materials. Intra-band scattering in different bands as well as inter-band scattering between the bands have a different influence on gap symmetry, transition

temperature, and resistivity, the latter losing its unambiguous indicator for the scattering strength.

A clear trend for the decrease in transition temperature was found in neutron irradiation experiments, i.e. $\Delta T_c \propto T_c$ at a given neutron fluence. Similar values for the normalized T_c reduction were obtained for various optimally doped iron-based compounds and the cuprates. It was only slightly smaller in the conventional superconductor Nb_3Sn. $\Delta T_c \propto T_c$ at a given fluence was also nearly independent of the doping level in K-doped Ba-122. However, contradicting results do exist, such as a larger decrease in strongly under- or over-doped crystals or the increase of T_c due to irradiation found for $FeSe_{1-x}Te_x$ or under-doped Ba-122. For a comparison of different materials and in particular different irradiation techniques, calculations of the number of displaced atoms would be desirable, but only a few data are currently available.

The upper critical field was not changed significantly in the majority of irradiation experiments on iron superconductors, data for changes of λ are scarce.

Flux pinning is similar in the cuprate and iron superconductors. Few crystals are very clean; many show a second peak effect. The latter disappears after irradiation to a sufficiently high fluence. In clean crystals on the other hand, the enhancement of J_c after irradiation can reach orders of magnitude.

It was pointed out that the depairing current is the material parameter defining the achievable currents after irradiation. A pinning efficiency, $\eta := J_c/J_d$, of around 0.03 was found for the neutron induced defect structure at self-field in all optimally doped Ba-122 crystals, which is consistent with available data on many cuprates. The 1111 family and K-doped Ba-122 are most promising for applications in this respect. A record low temperature self-field J_c was achieved in Sm-1111 by heavy ion irradiation, however, the smaller Ginzburg number of K-doped Ba-122 leads to a significantly weaker field and temperature dependence of J_c in this compound. The achievable currents by proton and neutron irradiation are similar. Higher currents were obtained with some (not all) high energy heavy ions. The latter resulted in a better in-field performance of J_c, which can be further improved by a combined proton and ion irradiation.

Acknowledgments

This work was supported by the Austrian Science Fund (FWF):I 2814-N36 and P 22837-N20. I wish to thank Hiroshi Eisaki, Shigeyuki Ishida, and Masamichi Nakajima from AIST as well as Ventsislav Mishev for the fruitful collaboration. Iron-based superconductors for our irradiation experiments were provided in addiation by NHFML (David Larbalestier, Jianyi Jiang, Jeremy Weiss, Eric Hellstrom, Akiyasu Yammoto), ETH Zurich (Janusz Karpinski, Nikolai Zhigadlo), NIMS (Yoshihiko Takano), and CNR-SPIN (Emilio Bellingeri, Marina Putti, Carlo Ferdeghini), which is gratefully acknowledged. Thanks to Daniel Kagerbauer for contributing data. I am grateful to Harald Weber for carefully proofreading the manuscript and fruitful discussions.

ORCID iDs

M Eisterer https://orcid.org/0000-0002-7160-7331

References

[1] Putti M, Affronte M, Ferdeghini C, Manfrinetti P, Tarantini C and Lehmann E 2006 *Phys. Rev. Lett.* **96** 077003
[2] Putti M *et al* 2010 *Supercond. Sci. Technol.* **23** 034003
[3] Jun-ichi S 2014 *Supercond. Sci. Technol.* **27** 044002
[4] Pallecchi I, Eisterer M, Malagoli M and Putti M 2015 *Supercond. Sci. Technol.* **28** 114005
[5] Leroux M *et al* 2015 *Appl. Phys. Lett.* **107** 192601
[6] Rupich M W *et al* 2016 *IEEE Trans. Appl. Supercond.* **26** 1–4
[7] Tönies S, Weber H W, Guo Y C, Dou S X, Sawh R and Weinstein R 2001 *Appl. Phys. Lett.* **78** 3851
[8] Eisterer M, Zehetmayer M, Weber H W, Jiang J, Weiss J D, Yamamoto A, Hellstrom E E, Larbalestier D C, Zhigadlo N D and Karpinski J 2010 *Supercond. Sci. Technol.* **23** 054006
[9] Hecher J, Baumgartner T, Weiss J D, Tarantini C, Yamamoto A, Jiang J, Hellstrom E E, Larbalestier D C and Eisterer M 2016 *Supercond. Sci. Technol.* **29** 025004
[10] Prokopec R, Fischer D X, Weber H W and Eisterer M 2015 *Supercond. Sci. Technol.* **28** 014005
[11] Emhofer J, Eisterer M and Weber H W 2013 *Supercond. Sci. Technol.* **26** 035009
[12] Jirsa M, Rameš M, Ďuran I, Melíšek T, Kováč P and Viererbl L 2017 *Supercond. Sci. Technol.* **30** 045010
[13] Baumgartner T, Eisterer M, Weber H W, Flükiger R, Scheuerlein C and Bottura L 2014 *Supercond. Sci. Technol.* **27** 015005
[14] Spina T, Scheuerlein C, Richter D, Ballarino A, Cerutti F, Esposito L S, Lechner A, Bottura L and Flükiger R 2016 *IEEE Trans. Appl. Supercond.* **26** 1–5
[15] Tarantini C *et al* 2010 *Phys. Rev. Lett.* **104** 087002
[16] Kraus M, Leghissa M and Saemann-Ischenko G 1994 *Phys. Bl.* **50** 333
[17] Nakajima Y, Tsuchiya Y, Taen T, Tamegai T, Okayasu S and Sasase M 2009 *Phys. Rev.* B **80** 012510
[18] Tamegai T *et al* 2012 *Supercond. Sci. Technol.* **25** 084008
[19] Fang L *et al* 2012 *Appl. Phys. Lett.* **101** 012601
[20] Civale L, Marwick A D, McElfresh M W, Worthington T K, Malozemoff A P, Holtzberg F H, Thompson J R and Kirk M A 1990 *Phys. Rev. Lett.* **65** 1164
[21] Matsui H, Ootsuka T, Ogiso H, Yamasaki H, Sohma M, Yamaguchi I, Kumagai T and Manabe T 2016 *Supercond. Sci. Technol.* **29** 065002
[22] Teknowijoyo S *et al* 2016 *Phys. Rev.* B **94** 064521
[23] Moore J D *et al* 2009 *Supercond. Sci. Technol.* **22** 125023
[24] Haberkorn N, Maiorov B, Usov I O, Weigand M, Hirata W, Miyasaka S, Tajima S, Chikumoto N, Tanabe K and Civale L 2012 *Phys. Rev.* B **85** 014522
[25] Weber H W, Böck H, Unfried E and Greenwood L R 1986 *J. Nucl. Mater.* **137** 236
[26] Frischherz M C, Kirk M A, Farmer J, Greenwood L R and Weber H W 1994 *Physica* C **232** 309
[27] Chudy M, Eisterer M, Weber W H, Veterníková J, Sojak S and Slugeň V 2012 *Supercond. Sci. Technol.* **25** 075017

[28] Krusin-Elbaum L, Thompson J R, Wheeler R, Marwick A D, Li C, Patel S, Shaw D T, Lisowski P and Ullmann J 1994 *Appl. Phys. Lett.* **64** 3331–3
[29] Weinstein R, Sawh R, Ren Y, Eisterer M and Weber H W 1998 *Supercond. Sci. Technol.* **11** 959
[30] Eisterer M, Tönies S, Novak W, Weber H W, Weinstein R and Sawh R 1998 *Supercond. Sci. Technol.* **11** 1001
[31] Zehetmayer M, Eisterer M, Jun J, Kazakov S M, Karpinski J, Birajdar B, Eibl O and Weber H W 2004 *Phys. Rev.* B **69** 054510
[32] Eisterer M, Weber H W, Jiang J, Weiss J D, Yamamoto A, Polyanskii A A, Hellstrom E E and Larbalestier D C 2009 *Supercond. Sci. Technol.* **22** 065015
[33] Mizukami Y *et al* 2014 *Nat. Commun.* **5** 5657
[34] Salovich N W *et al* 2013 *Phys. Rev.* B **87** 180502
[35] Strehlow C P, Kończykowski M, Murphy J A, Teknowijoyo S, Cho K, Tanatar M A, Kobayashi T, Miyasaka S, Tajima S and Prozorov R 2014 *Phys. Rev.* B **90** 020508
[36] Taen T, Ohtake F, Akiyama H, Inoue H, Sun Y, Pyon S, Tamegai T and Kitamura H 2013 *Phys. Rev.* B **88** 224514
[37] Schilling M B *et al* 2016 *Phys. Rev.* B **93** 174515
[38] Dong J K, Zhou S Y, Guan T Y, Zhang H, Dai Y F, Qiu X, Wang X F, He Y, Chen X H and Li S Y 2010 *Phys. Rev. Lett.* **104** 087005
[39] Reid J-P *et al* 2012 *Phys. Rev. Lett.* **109** 087001
[40] Wang A F *et al* 2014 *Phys. Rev.* B **89** 064510
[41] Karkin A E, Werner J, Behr G and Goshchitskii B N 2009 *Phys. Rev.* B **80** 174512
[42] Kim J *et al* 2012 *Phys. Rev.* B **86** 144509
[43] Nakajima Y, Taen T, Tsuchiya Y, Tamegai T, Kitamura H and Murakami T 2010 *Phys. Rev.* B **82** 220504
[44] Prozorov R, Kończykowski M, Tanatar M A, Thaler A, Bud'ko S L, Canfield P C, Mishra V and Hirschfeld P J 2014 *Phys. Rev.* X **4** 041032
[45] Weaver B D 2014 *Physica* C **501** 36
[46] Mazin I I, Singh D J, Johannes M D and Du M H 2008 *Phys. Rev. Lett.* **101** 057003
[47] Efremov D V, Korshunov M M, Dolgov O V, Golubov A A and Hirschfeld P J 2011 *Phys. Rev.* B **84** 180512
[48] Wang Y, Kreisel A, Hirschfeld P J and Mishra V 2013 *Phys. Rev.* B **87** 094504
[49] Cho K, Konczykowski M, Murphy J, Kim H, Tanatar M A, Straszheim W E, Shen B, Wen H H and Prozorov R 2014 *Phys. Rev.* B **90** 104514
[50] Das T, Zhu J-X and Graf M J 2011 *Phys. Rev.* B **84** 134510
[51] Bang Y, Choi H-Y and Won H 2009 *Phys. Rev.* B **79** 054529
[52] Kogan V G and Prozorov R 2016 *Phys. Rev.* B **93** 224515
[53] Hirschfeld P J, Korshunov M M and Mazin I I 2011 *Rep. Prog. Phys.* **74** 124508
[54] Kang J and Fernandes R M 2016 *Phys. Rev.* B **93** 224514
[55] Li Y, Shen C, Luo Y, Yang X, Tao Q, Cao G H and Xu U-A 2013 *Europhys. Lett.* **102** 37003
[56] Testardi L R and Mattheiss L F 1978 *Phys. Rev. Lett.* **41** 1612–5
[57] Putti M, Brotto P, Monni M, Galleani E, Sanna A and Massidda S 2007 *Europhys. Lett.* **77** 57005
[58] Kihlstrom K J *et al* 2013 *Appl. Phys. Lett.* **103** 202601
[59] Ozaki T, Wu L, Zhang C, Jaroszynski J, Si W, Zhou J, Zhu Y and Li Q 2016 *Nat. Commun.* **7** 13036
[60] Mishev V, Eisterer M and Takana Y private communication
[61] Mizukami Y, Konczykowski M, Matsuura K, Watashige T, Kasahara S, Matsuda Y and Shibauchi T 2017 *J. Phys. Soc. Japan* **86** 083706
[62] Eisterer M, Fuger R, Chudy M, Hengstberger F and Weber H W 2010 *Supercond. Sci. Technol.* **23** 014009
[63] Werner M, Sauerzopf F M, Weber H W and Wisniewski A 2000 *Phys. Rev.* B **61** 14795–803
[64] Sauerzopf F M, Wiesinger H P, Kritscha W, Weber H W, Crabtree G W and Liu J Z 1991 *Phys. Rev.* B **43** 3091
[65] Baumgartner T, Eisterer M, Weber H W, Flükiger R, Scheuerlein C and Bottura L 2014 *Sci. Rep.* **5** 10236
[66] Spina T, Scheuerlein C, Richter D, Bordini B, Bottura L, Ballarino A and Flükiger R 2015 *IEEE Trans. Appl. Supercond.* **25** 1–5
[67] Flükiger R *et al* 2017 *Supercond. Sci. Technol.* **30** 054003
[68] Kagerbauer D, Mishev V, Ishida S, Song D J, Ogino H, Eisaki H, Nakajima M and Eisterer M 2017 Poster Presentation at EUCAS
[69] Cho K *et al* 2016 *Sci. Adv.* **2** e1600807
[70] Mishev V, Nakajima M, Eisaki H and Eisterer M 2016 *Sci. Rep.* **6** 27783
[71] Maiorov B, Katase T, Usov I O, Weigand M, Civale L, Hiramatsu H and Hosono H 2012 *Phys. Rev.* B **86** 094513
[72] Salem-Sugui S, Moseley D, Stuard S J, Alvarenga A D, Sefat A S, Cohen L F and Ghivelder L 2017 *J. Alloys Compd.* **694** 1371–5
[73] Taen T, Nakajima Y, Tamegai T and Kitamura H 2012 *Phys. Rev.* B **86** 094527
[74] Haberkorn N, Kim J, Gofryk K, Ronning F, Sefat A S, Fang L, Welp U, Kwok W K and Civale L 2015 *Supercond. Sci. Technol.* **28** 055011
[75] Yagyuda H, Nakajima Y, Tamegai T, Kanai Y and Kambara T 2011 *Physica* C **471** 790
[76] Taen T, Ohtake F, Pyon S, Tamegai T and Kitamura H 2015 *Supercond. Sci. Technol.* **28** 085003
[77] Park A *et al* 2016 *Supercond. Sci. Technol.* **29** 055006
[78] Ahmad D, Seo Y I, Choi W J and Kwon Y S 2017 *Supercond. Sci. Technol.* **30** 025009
[79] Eisterer M, Mishev V, Zehetmayer M, Zhigadlo N D, Katrych S and Karpinski J 2014 *Supercond. Sci. Technol.* **27** 044009
[80] Tarantini C *et al* 2010 *Appl. Phys. Lett.* **96** 142510
[81] Eisterer M, Raunicher R, Weber H W, Bellingeri E, Cimberle M R, Pallecchi I, Putti M and Ferdeghini C 2011 *Supercond. Sci. Technol.* **24** 065016
[82] Bellingeri E *et al* 2012 *Supercond. Sci. Technol.* **25** 084022
[83] Haigh S, Kovac P, Prikhna T A, Savchuk Y M, Kilburn M R, Salter C, Hutchison J and Grovenor C 2005 *Supercond. Sci. Technol.* **18** 1190
[84] Eisterer M 2007 *Supercond. Sci. Technol.* **20** R47
[85] Eisterer M, Müller R, Schöppl R, Weber H W, Soltanian S and Dou S X 2007 *Supercond. Sci. Technol.* **20** 117
[86] Eisterer M, Zehetmayer M, Weber H W, Jiang J, Weiss J D, Yamamoto A and Hellstrom E E 2009 *Supercond. Sci. Technol.* **22** 095011
[87] Fang L *et al* 2013 *Nat. Commun.* **4** 2655
[88] Giamarchi T and Le Doussal P 1997 *Phys. Rev.* B **55** 6577–83
[89] Mikitik G P and Brandt E H 2001 *Phys. Rev.* B **64** 184514
[90] Brandstätter G, Sauerzopf F M and Weber H W 1997 *Phys. Rev.* B **55** 11693–701
[91] Weigand M, Eisterer M, Giannini E and Weber H W 2010 *Phys. Rev.* B **81** 014516
[92] Gordon R T *et al* 2010 *Phys. Rev.* B **82** 054507
[93] Williams T J *et al* 2009 *Phys. Rev.* B **80** 094501
[94] Williams T J *et al* 2010 *Phys. Rev.* B **82** 094512
[95] Luan L, Lippman T M, Hicks C W, Bert J A, Auslaender O M, Chu J-H, Analytis J G, Fisher I R and Moler K A 2011 *Phys. Rev. Lett.* **106** 067001
[96] Ofer O *et al* 2012 *Phys. Rev.* B **85** 060506
[97] Ishida S, Song D, Ogino H, Iyo A, Eisaki H, Nakajima M, Shimoyama J-i and Eisterer M 2017 *Phys. Rev.* B **95** 014517

[98] Hashimoto K *et al* 2012 *Science* **336** 1554–7
[99] Diao Z, Campanini D, Fang L, Kwok W-K, Welp U and Rydh A 2016 *Phys. Rev.* B **93** 014509
[100] Li G, Hu W Z, Dong J, Li Z, Zheng P, Chen G F, Luo J L and Wang N L 2008 *Phys. Rev. Lett.* **101** 107004
[101] Hiraishi M, Kadono R, Soshi Takeshita S, Miyazaki M, Koda A, Okabe H and Akimitsu J 2009 *J. Phys. Soc. Japan* **78** 023710
[102] Khasanov R, Luetkens H, Amato A, Klauss H-H, Ren Z-A, Yang J, Lu W and Zhao Z-X 2008 *Phys. Rev.* B **78** 092506
[103] Drew A J *et al* 2008 *Phys. Rev. Lett.* **101** 097010
[104] Weyeneth S, Puzniak R, Zhigadlo N D, Katrych S, Bukowski Z, Karpinski J and Keller H 2009 *J. Supercond. Novel Magn.* **22** 347–51
[105] Welp U, Chaparro C, Koshelev A E, Kwok W K, Rydh A, Zhigadlo N D, Karpinski J and Weyeneth S 2011 *Phys. Rev.* B **83** 100513
[106] Biswas P K, Balakrishnan G, Paul D M, Tomy C V, Lees M R and Hillier A D 2010 *Phys. Rev.* B **81** 092510
[107] Kim H *et al* 2010 *Phys. Rev.* B **81** 180503
[108] Klein T *et al* 2010 *Phys. Rev.* B **82** 184506
[109] Prozorov R, Tanatar M A, Roy B, Ni N, Bud'ko S L, Canfield P C, Hua J, Welp U and Kwok W K 2010 *Phys. Rev.* B **81** 094509
[110] Fang L, Jia Y, Schlueter J A, Kayani A, Xiao Z L, Claus H, Welp U, Koshelev A E, Crabtree G W and Kwok W-K 2011 *Phys. Rev.* B **84** 140504
[111] Mishev V, Zehetmayer M, Fischer D X, Nakajima M, Eisaki H and Eisterer M 2015 *Supercond. Sci. Technol.* **28** 102001
[112] Blatter G, Geshkenbein V B and Larkin A I 1992 *Phys. Rev. Lett.* **68** 875
[113] Sun Y, Pyon S, Tamegai T, Kobayashi R, Watashige T, Kasahara S, Matsuda Y, Shibauchi T and Kitamura H 2015 *Appl. Phys. Express* **8** 113102